6-27-2014

Recent Changes in Central and Eastern Pacific El Niño

Peter M. Washam
pwash005@fiu.edu

FLORIDA INTERNATIONAL UNIVERSITY

Miami, Florida

RECENT CHANGES IN CENTRAL AND EASTERN PACIFIC EL NIÑO

A thesis submitted in partial fulfillment of

requirements for the degree of

MASTER OF SCIENCE

in

GEOSCIENCES

by

Peter Marshall Washam

2014

To: Interim Dean Michael R. Heithaus
College of Arts and Sciences

This thesis, written by Peter Marshall Washam, and entitled Recent Changes in Central and Eastern Pacific El Niño, having been approved in respect to style and intellectual content, is referred to you for judgment.

We have read this thesis and recommend that it be approved.

_____
Ping Zhu

_____
Hugh Willoughby

_____
Ben Kirtman

_____
Robert Burgman, Major Professor

Date of Defense: June 27, 2014

The thesis of Peter Marshall Washam is approved.

_____
Interim Dean Michael R. Heithaus
Interim Dean, College of Arts and Sciences

_____
Dean Lakshmi N. Reddi
University Graduate School

Florida International University, 2014

ACKNOWLEDGMENTS

I would like to thank my advisor Dr. Robert Burgman for his patience, vision, and guidance during the process of completing my thesis. I am equally grateful for the wisdom imparted to me by Dr. Burgman pertaining to the process of growing into a well-spoken scientist. Dr. Burgman's influence cannot be understated.

I am grateful for the guidance that Dr. Ben Kirtman played in over-seeing the direction of research involved in my thesis.

I am equally grateful for my other two committee members: Dr. Ping Zhu and Dr. Hugh Willoughby for their insight throughout the process of writing my thesis document.

I would also like to thank Dr. You Kyung Jhang and Isaac Pei for their help with the writing and de-bugging of computer scripts.

I am eternally grateful for the love and support of my wife, Elizabeth as well as my mother, Betsy, my father, Roy, my brother, Ethan, and my sister, Grace.

Finally, I would like to thank the whole Earth and Environment department of Florida International University for making the past two years a positive experience.

ABSTRACT OF THE THESIS

RECENT CHANGES IN CENTRAL AND EASTERN PACIFIC EL NIÑO

by

Peter Marshall Washam

Florida International University, 2014

Miami, Florida

Professor Robert Burgman, Major Professor

Recent research indicates that characteristics of El Niño and the Southern Oscillation (ENSO) have changed over the past several decades. Here, I examined different flavors of El Niño in the observational record and the recent changes in the character of El Niño events. The fundamental physical processes that drive ENSO were described and the Eastern Pacific (EP) and Central Pacific (CP) types or flavors of El Niño were defined. Using metrics from the peer-reviewed literature, I examined several historical data sets to interpret El Niño behavior from 1950-2010. A Monte Carlo Simulation was then applied to output from coupled model simulations to test the statistical significance of recent observations surrounding EP and CP El Niño. Results suggested that EP and CP El Niño had been occurring in a similar fashion over the past 60 years with natural variability, but no significant increase in CP El Niño behavior.

TABLE OF CONTENTS

LIST OF FIGURES

ABBREVIATIONS AND SYMBOLS

Central Pacific (El Niño)	CP
The Delayed Oscillator	DO
El Niño Modoki Index	EMI
El Niño Southern Oscillation	ENSO
Eastern Pacific (El Niño)	EP
National Oceanic and Atmospheric Administration	NOAA
Pacific Decadal Oscillation	PDO
Pre-industrial Control	Pi-control
Precipitation Anomaly	PrecipA
Surface Air Temperature Anomaly	SATA
Sea Surface Temperature (Anomaly)	SST(A)
Sub-surface Temperature Anomaly	SubSTA
Trans Niño Index	TNI
Standard Deviation	σ
Variance	σ^2

CHAPTER 1

INTRODUCTION

El Niño and the Southern Oscillation, or ENSO, describes a coupled ocean atmosphere phenomenon that originates in the equatorial Pacific and affects regional and global climate on inter-annual timescales. The term Southern Oscillation was coined by Walker and Bliss (1932) to describe a "seesaw" in the sea level pressure (SLP) that occurs across the equatorial Pacific affecting rainfall patterns and wind fields. Walker and Bliss (1932) found that when pressure is high over the Pacific Ocean it tends to be low over the Indian Ocean. Multiple regions in both the Northern and Southern Hemisphere were investigated to support their hypothesis. Bjerknes (1966,1969) later included the Southern Oscillation within a basin wide phenomenon involving ocean and atmospheric interactions. It was found that when large sea surface temperature (SST) anomalies extend over an equatorial zone from South America to the mid-Pacific, there is a weakening of equatorial easterly winds and low atmospheric pressure. The warming was found to stem from weakening or complete termination of oceanic upwelling in the region. The ocean components of ENSO are referred to as El Niño and La Niña and are commonly described by the area averaged SST anomalies in the Niño 3.4 region (5°N–5°S, 170°–120°W).

Figure 1 shows the historical variations of the SST anomalies in the Niño 3.4 region.

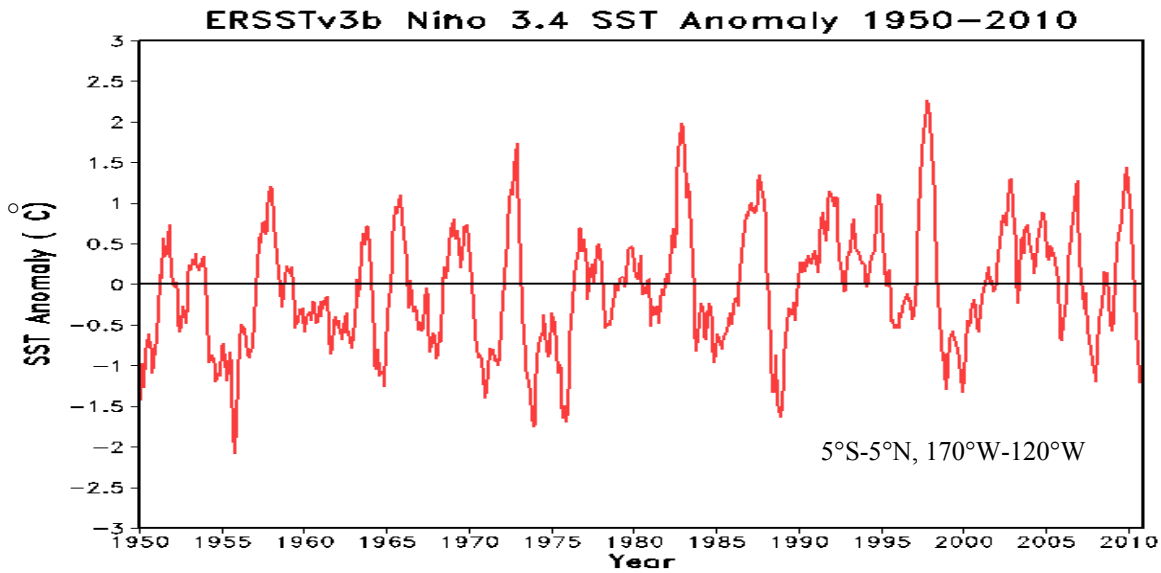

Figure 1. ERSSTv3b Niño 3.4 SST Anomaly 1950-2010. Sea Surface Temperature Anomalies (SSTAs) in the Niño 3.4 region from 1950-2010 calculated from ERSSTv3b using a seasonal climatology based on the 1971-2000 time period. SSTAs in °C.

Figure 2 shows the Niño 3.4 region and other regions used to measure ENSO characteristics. Positive values correspond with the warm phase or El Niño conditions while negative values indicate cool or La Niña conditions.

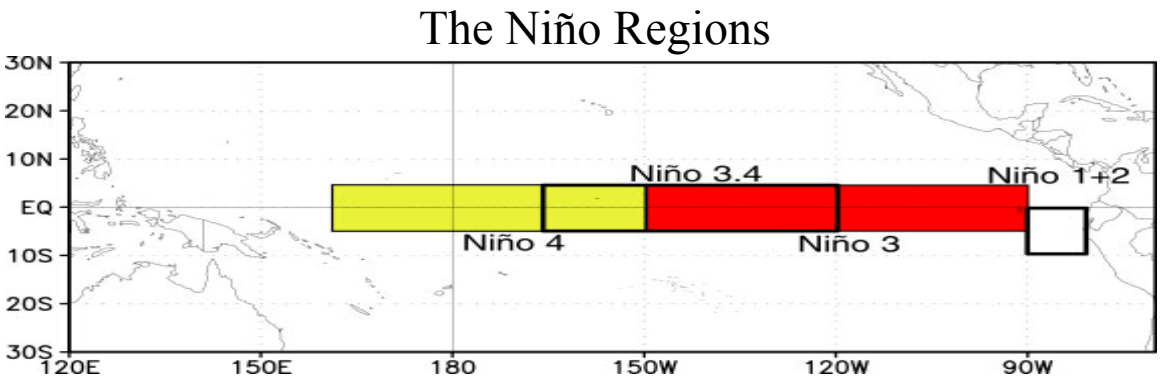

Figure 2. The Niño Regions. The Niño regions (1+2, 3, 3.4, 4) are a set of area averaged SSTAs that are used as indices in order to track the evolution of ENSO. Picture from: http://www.cpc.ncep.noaa.gov/products/analysis_monitoring/ensostuff/nino_regions.shtml.

The oscillatory nature of ENSO is clearly illustrated in Figure 1 and a description of El Niño and La Niña events first requires a description of "normal" conditions in the Pacific as described by the time average. Normal conditions in the equatorial Pacific find

easterly trade winds near the surface, deep convection over the warmest surface waters in the west, westerly winds aloft, and subsidence over the cooler waters of the east Pacific. The zonal circulation pattern described above is called the Walker Circulation and is intimately tied to the underlying ocean (Sheinbaum, 2003). The surface easterlies induce poleward Ekman transport in the ocean near the equator, providing the proper environment for equatorial upwelling in the eastern Pacific resulting in a shallow thermocline and a "cold tongue" at the surface. In the western Pacific, advection of warm tropical waters by the easterly trades result in a vast region of warm surface waters or "warm pool" and a deep thermocline. The east west SST gradient further enhances the easterly flow of the trades.

Bjerknes (1969) argued that the onset of an El Niño event was the result of to a positive feedback between the surface winds, the equatorial thermocline, and the SST gradient near the equator. The canonical El Niño onset occurs when the easterly trades weaken for a period of time, allowing the warm waters of the western Pacific to shift to the east. As the relatively cool surface waters of the central and eastern Pacific experience warming, the climatological temperature gradient along the equator decreases, resulting in a further weakening of the trade winds. In the west, the shifting waters result in a shallower thermocline while in the east, the weaker trades reduce upwelling and the thermocline deepens.

Figure 3 shows the SST anomalies associated with the 1997-98 El Niño event. The anomalously warm surface waters extend from the coast of South America westward into the central equatorial Pacific while the waters of the west Pacific "Warm Pool" tend to experience anomalous cooling. In the atmosphere, the Walker circulation weakens as

the region of deep convection shifts to the east. The opposite occurs during the cold phase of the Oscillation (La Niña). La Niña conditions are characterized by an intensification of the climatological Walker circulation (Sheinbaum, 2003). The warm surface waters of the west Pacific intensify and spread westward while SSTs in the east Pacific Ocean cool and the thermocline shoals. The Bjerknes feedback provides a physically consistent explanation of the growth of an El Niño event, but does not address the reversal of the departure from normal conditions necessary to describe the oscillatory behavior observed in Figure 1 (Sheinbaum, 2003). For this there must be a mechanism for the termination of the positive feedback process.

1.1 Mechanisms

The literature points to several possible mechanisms for the behavior of ENSO over the period of observations that involve both oceanic and atmospheric dynamics In this section we briefly describe three such mechanisms.

The Delayed Oscillator

The Delayed Oscillator theory (Schopf and Suarez, 1988) seeks to describe the mechanism of termination of an ENSO event through ocean wave dynamics. To understand the Delayed Oscillator one can assume a simplified tropical Pacific Ocean with water temperatures that vary only with depth and a constant thermocline throughout. The motionless ocean basin is perturbed by initiating some isolated westerly (eastward) wind stress around the equator in the central part of the simplified ocean resulting in the creation of two types of equatorial waves. At the equator, a westerly wind perturbation creates a downwelling Kelvin wave that travels eastward at a speed of ~3m/s, deepening

the thermocline and warming the surface layer. Poleward of the initial equatorial perturbation a pair of upwelling Rossby waves is created and propagates westward at a slower speed (~1 m/s), causing the thermocline to shoal and the surface layer to cool. When the faster moving Kelvin wave reaches the eastern boundary of the simplified ocean, contact with the eastern boundary will result in two coastally trapped Kelvin waves that propagate poleward in both hemispheres and the reflection of two westward propagating down welling Rossby waves. The upwelling Rossby waves created by the original wind perturbation eventually reach the western boundary and reflect an upwelling Kelvin wave that travels eastward, carrying with it the cooler equatorial waters that terminate the warm event in the east. The simplified model of the Delayed Oscillator is an idealized description of the oceanic response to a single event of wind stress and proves to be informative. However, in nature wind stress and ocean waves are continuous and the time scales of the ENSO event are much longer.

The Recharge-Discharge Oscillator

The Recharge-Discharge Oscillator is built upon results from Cane and Zebiak (1985), who argued that ENSO was related to equatorial heat content identified by thermocline depth. Proposed by Jin (1997), the model states that during the warm phase, westerly wind anomalies produce warm SSTs in the eastern Pacific. Off-equatorial Rossby waves move subsurface water poleward via Sverdrup transport, which exports heat from the equator. Once exhausted, the equatorial thermocline becomes shallower, cold SSTs return to the eastern Pacific, and the cold phase is initiated. Easterly wind anomalies then produce a meridional Sverdrup transport that replenishes the equatorial heat content, deepening the thermocline and repeating the cycle once more.

The Advective-Reflective Oscillator

Picaut et al. (1997) sought to describe El Niño by focusing on the advection produced by the reflection of signals off of eastern and western boundaries taking the form of equatorial ocean waves. Here, the termination of an El Niño is presented as a result of a negative feedback mechanism containing an upwelling Kelvin wave and downwelling Rossby waves. Both the Kelvin waves and the Rossby waves produce westward anomalous currents, that pair with mean zonal currents to return warm SSTs to the west Pacific.

1.2 ENSO Characteristics

Phase Locking to the Seasonal Cycle

Canonical El Niño and La Niña events tend to develop in late boreal spring and summer months, mature near the end of the calendar year, and decay rapidly by the following summer. The "phase locking" of ENSO with the seasonal cycle points to a strong influence of the changing strength of the ocean-atmosphere coupling strength via changes of upwelling, ITCZ location, and surface winds (ocean waves) over the seasonal cycle on the coupled instability that drives ENSO. For a thorough discussion of this topic see Galanti and Tziperman (2000).

ENSO Irregularity in time

The time series of Niño 3.4 shown in Figure 1 indicates that the amplitude and frequency of ENSO change over time. Irregularity in the behavior of ENSO on decadal timescales has lead to a debate in the literature as to the processes responsible for ENSO development and variability. One theory characterizes ENSO as a stable stochastically

forced phenomenon where ENSO growth and variability is determined by atmospheric dynamics (Penland and Sardeshmukh, 1995; Ping et al., 1996). Others argue that ENSO can be described as an unstable self-sustained mode of variability where irregularity is a result of interactions with other modes of variability such as the seasonal cycle or decadal variations in the climatological mean state of the tropical Pacific caused by ocean atmosphere dynamics in the tropics or midlatitudes (Zebiak, 1989; Burgman et al., 2008). In the unstable ENSO regime, stochastic forcing may play a significant role in the modulating of ENSO variability and predictability (Kirtman and Schopf 1998). Whether the oscillation itself is damped and stochastically forced, or it is a chaotic system containing an irregularity within, predictability remains a challenge. Prediction of ENSO is of great importance to society because of the extent of ENSO impacts worldwide via teleconnections.

Irregularity in space or Flavors of El Niño

Until recently, ENSO has been considered as a single phenomenon, and as such, was defined using a single metric. As stated by the National Oceanic and Atmospheric Administration (NOAA): "El Niño can be said to occur if sea surface temperature anomalies (SSTAs) in the Niño 3.4 region (5°N–5°S, 120°–170°W) exceed or equal 0.5 C° for a period of at least five consecutive overlapping three-month seasons based on a 1971-2000 climatology (http://www.climate.gov/news-features/understanding-climate/watching-el-ni%C3%B1o-and-la-ni%C3%B1a-noaa-adapts-global-warming)." Trenberth and Stepaniak (2001) argued that in order to capture the many "flavors" of ENSO, more than one index was required. When Ashok et al. (2007) applied an empirical orthogonal function analysis to observational data from 1979-2005 they found ENSO

events with different spatial characteristics in the central Pacific. Because the phenomenon was determined to be unrelated to ENSO evolution it was labeled ENSO Modoki (pseudo-El Niño). Since that time, much research has been focused on the differences between the Central Pacific (CP) El Niño and the canonical Eastern Pacific (EP) El Niño.

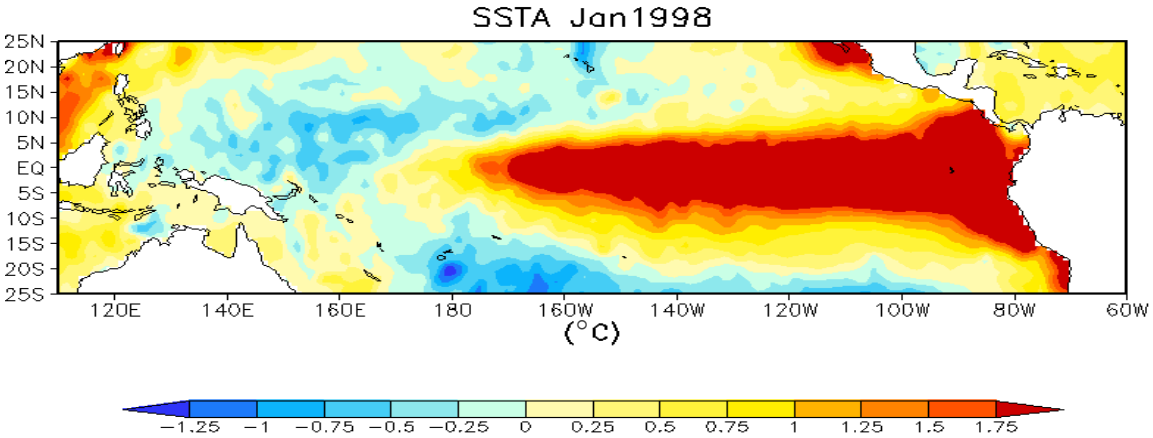

Figure 3. SSTA Jan1998. January 1998 Sea Surface Temperature Anomaly during a mature EP El Niño. Calculated using HadISST1 with a 1971-2000 seasonal climatology. SSTAs in °C

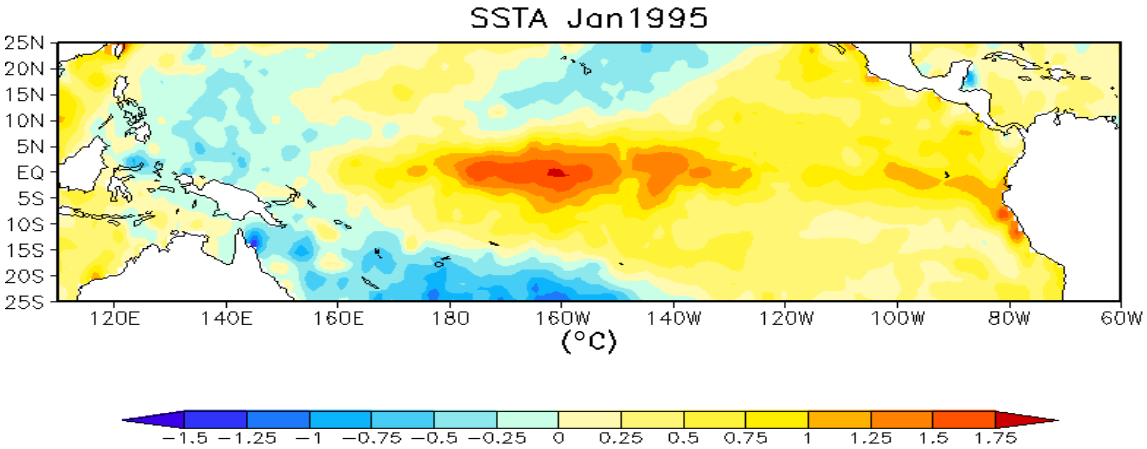

Figure 4. SSTA Jan1995. January 1995 Sea Surface Temperature Anomaly during a mature CP El Niño. Calculated using HadISST1 with a 1971-2000 seasonal climatology. SSTA in °C.

Figure 3 illustrates the spatial structure of a mature EP El Niño. Figure 4 reveals the spatial structure of a mature CP El Niño.

(a)

EP El Niño SSTA Evolution

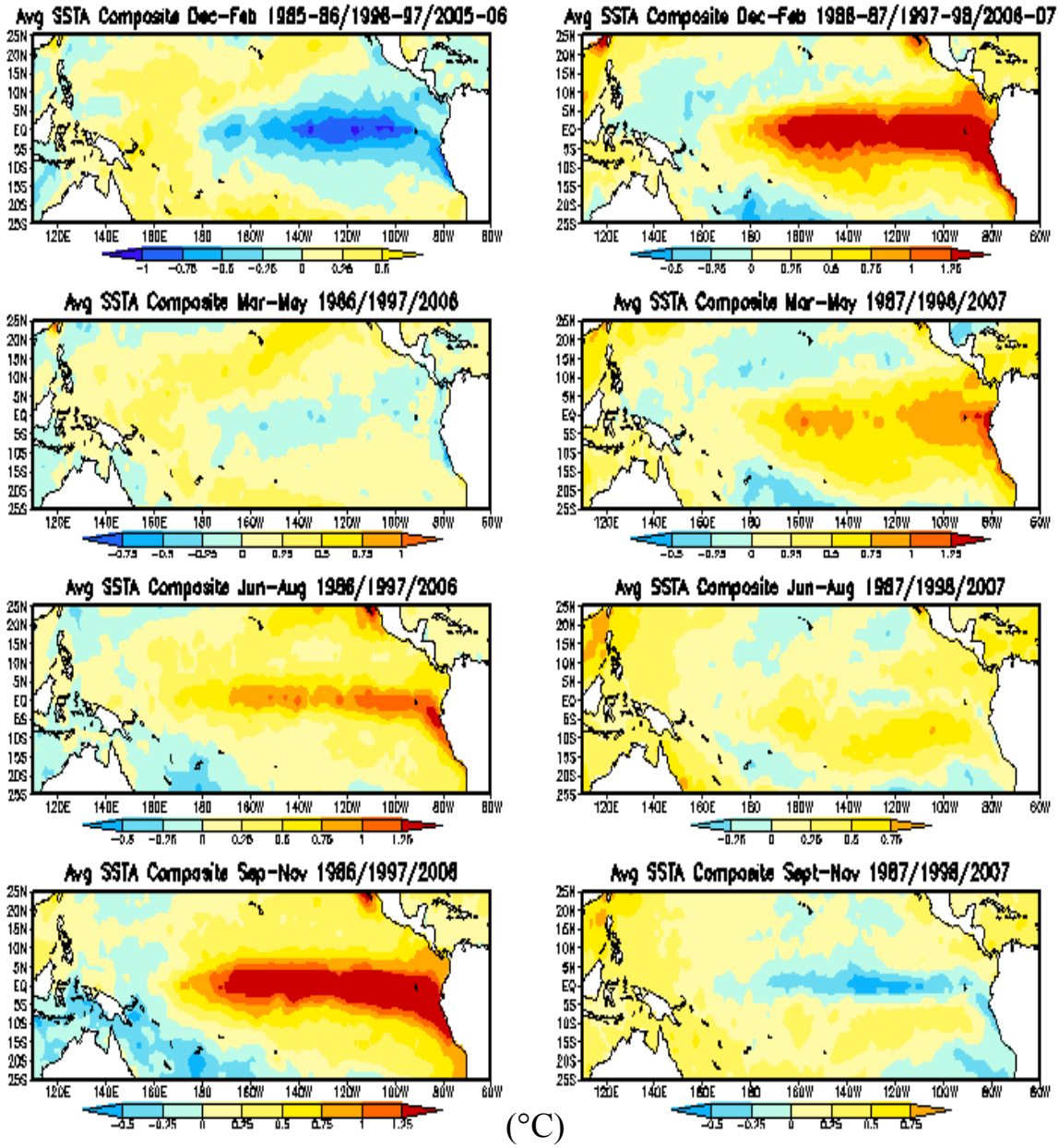

(°C)

(b)

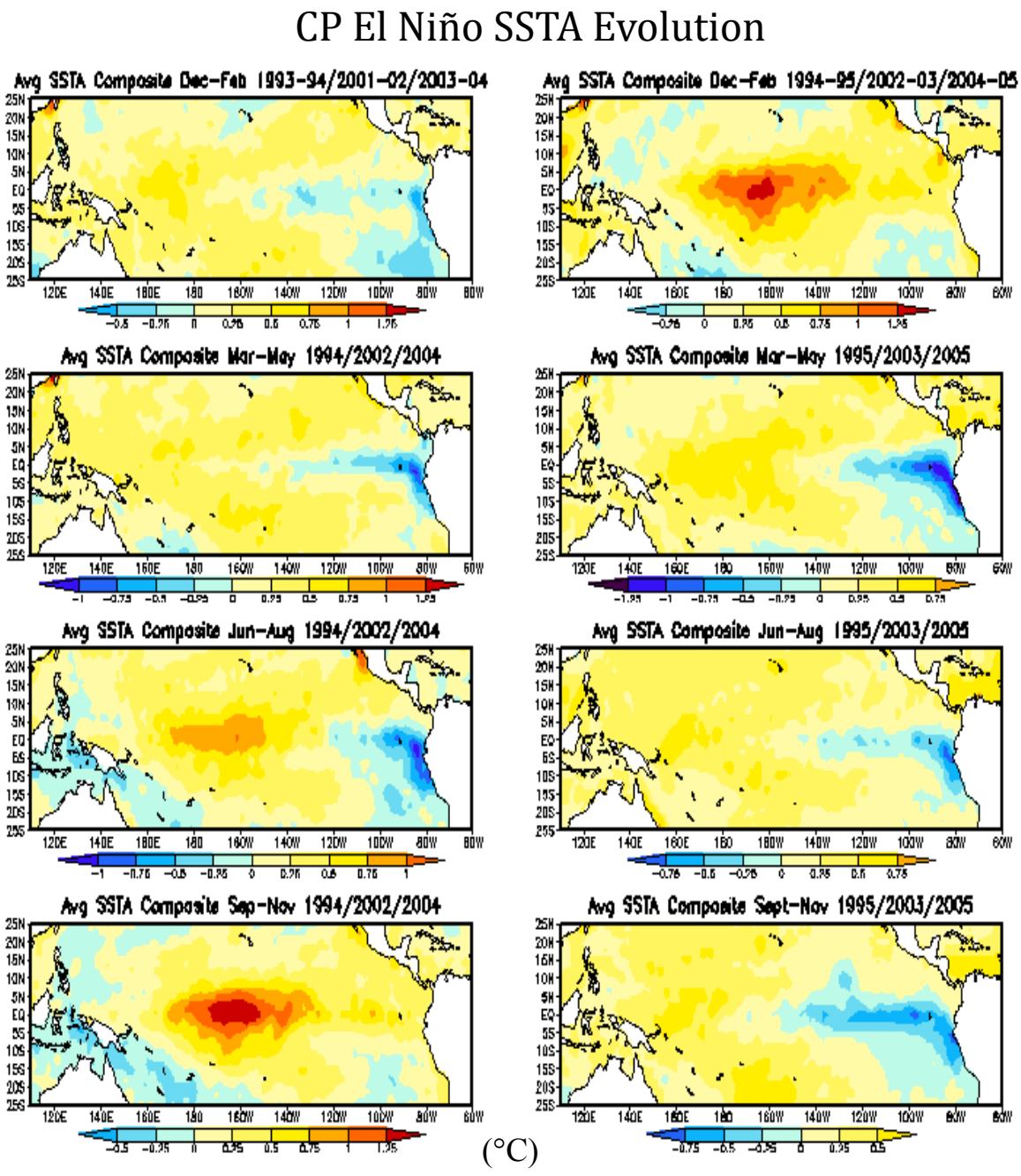

Figure 5. (a) EP El Niño SSTA Evolution. (b) CP El Niño SSTA Evolution. 3 month averages of SST anomalies demonstrating propagation of (a) Composite of EP El Niño events: 1986/87, 1997/98, 2006/07, and (b) Composite of CP El Niño events: 1994/95, 2001/02, 2004/05. Calculated using HadISST1 with a 1971-2000 seasonal climatology. SSTAs in °C.

Figure 5 displays the Composite average SST anomaly of 3 EP (a) and 3 CP (b) El Niño events over the period of their evolution. During an EP El Niño positive SSTAs originate along the western coast of South America (Niño 1+2) in March. The warm anomalies extend westward to the Niño 3 region in April, then to Niño 3.4 in May, and finally to Niño 4 during September. SSTAs peak during Boreal Winter, before retreating in an almost identically opposite fashion that restores the normal cold waters of the eastern Pacific "cold tongue." Typically, the Niño regions experience this decay in April of the second year with the exception of the Niño 1+2 region, which decays in July (Kao and Yu, 2009).

The CP El Niño has a different structure. Positive SST anomalies often begin during the summer months near the international dateline (180° longitude), mature during December and January, and retreat during spring of the second year. The anomalies associated with CP El Niño spread meridionally, but fail to propagate zonally to the extent that EP El Niño does. Figure 4b reveals that these warm ocean anomalies are more ambiguous than those of EP El Niño with small patches of warm water occurring in the eastern Pacific during the fall and winter months. Furthermore, Figure 5 demonstrates that CP (EP) El Niño events are characterized by weaker (stronger) SSTAs with maximum composite values around +1.25 °C (+2.0 °C), and have a shorter (longer) duration of around 9 (15) months.

Kao and Yu (2009) studied both sea surface and sub-surface temperature anomalies (SubSTA) for CP and EP types of El Niño. They found that positive SubSTAs extend deeper in the water column for EP El Niño, whereas CP El Niño events are initated at the surface with shallow SubSTAs. Yu and Kim (2010) found that while

thermocline processes may control the generation of the EP type of El Niño, they only determine the period of decay for CP El Niño events. The result of Yu and Kim (2010) supports the argument that the processes controlling the evolution of these two types of El Niño must be different.

Kug et al. (2009) investigated the governing mechanisms for Warm Pool El Niño (another name for CP El Niño) using observational SST and atmospheric data. They found that much different than its cousin in the eastern Pacific, CP El Niño is not driven by thermocline variations, but instead through anomalous advection by surface currents, and the vertical temperature gradient supply and drive SSTA development in CP El Niño. Sea surface height leads subsurface warming and the eastward current, which both in turn lead surface warming. Once the surface warming initializes, the mean zonal and meridional currents propagate the anomaly eastward and poleward. Here CP El Niño SSTAs induce precipitation and wind stress anomalies that enhance the development of the event. In the mature phase, westward zonal advection of cold water induced by the change of sea surface height distribution acts to damp the event (Kug et al., 2009). Wind anomalies provide the mechanism that prevents the development of large SSTAs over the eastern Pacific. During a CP El Niño, the precipitation anomaly is located near the dateline, allowing for strong westerly wind stress anomalies to occur from 130˚E-160˚W (including Niño 4 region), but easterly wind stress anomalies to prevail over most of the Niño 3 region. The wind stress structure of a CP El Niño is governed by the dynamics presented in Gill (1982). An in-phase relation observed between precipitation and wind stress combines with the structure mentioned above to enhance the warm (cold) SSTA in the central (eastern) Equatorial Pacific by downwelling (upwelling). These convergent

winds play a significant role in both damping and containing positive SSTAs in the central Pacific. Thermocline feedback is the key process in EP El Niño, but zonal advective feedback largely controls development and decay of warm ocean anomalies present in CP El Niño.

The CP El Niño tends to occur more frequently during the warm phase of the 10-15 year Pacific Decadal Oscillation (PDO) (Kug et al., 2009). The interaction between the local atmospheric forcing and a warm PDO is important in relation to the resultant ocean warming from Climate Change. If long term warming of SSTs in the tropical Pacific is expected, CP El Niño will be an important player in regional climate changes worldwide. Thus, understanding and predicting teleconnections associated with CP El Niño is an essential skill to posses.

Teleconnections

El Niño Teleconnections are the result of anomalous warming in the equatorial Pacific Ocean on regional climates worldwide. Central Pacific and Eastern Pacific El Niño have different spatial SST anomaly structures, which result in different footprints on regional climates around the world. Ashok et al. (2007) thoroughly investigated teleconnections for EP El Niño and El Niño Modoki. The description of an El Niño Modoki is comparable to that of a CP El Niño, and for the purposes of this study they will be referred to as one and the same.

Boreal Summer

During Northern Hemisphere Summer, an EP El Niño results in positive rainfall anomalies over the eastern Pacific, with negative anomalies in the tropical western Pacific and equatorial South America. In North America, increases in precipitation are

favored over the Southwest and the Northwest from Washington up to Alaska, the Great Plains, as well as the East Coast, contrasted by negative anomalies around the central and western Gulf Coast. ENSO signals can also be seen in Indian, Australian, and other monsoon seasons. Eastern Pacific El Niño conditions can cause serious draught during boreal summer months in India and Australia, retarding the monsoon in these places (Mo, Schemm, and Yoo, 2009). EP El Niño also causes warm air temperatures along the Pacific coast of North America up to Alaska, Central and East Africa, and South Asia. Cool temperatures are found over northeastern North America, eastern China, Japan, the tropical western Pacific islands, Turkey, and southern Mediterranean Europe.

However, CP El Niño has a different footprint on regional climates worldwide. During CP El Niño boreal summers, positive precipitation anomalies are seen over the central equatorial Pacific bounded by negative rainfall anomalies in the East and West. Northern India receives wet conditions countered by drought in southern Japan, eastern Australia, and the western coast of North America. Central Pacific El Niño is associated with globally cool temperatures, expect for parts of South America.

Boreal Winter

An EP El Niño boreal winter causes drought over the western Pacific tropics and sub-tropics, countered by wet conditions in the central and eastern equatorial Pacific, northern Argentina, southeast Brazil, northeast Africa, and southeastern North America. EP El Niño causes warm air temperatures over global tropical regions with exception to the western tropical Pacific. Positive Surface Air Temperature (SAT) anomalies are also identified over eastern and southwestern Australia, Japan, and the South China Sea. Negative SATAs are found over New Zealand and inland Mexico.

During CP El Niño boreal winters, the eastern Pacific experiences drought along with southern Thailand, the Philippines, southern India, Sri Lanka, Northwest United States, and East Africa. Central Pacific El Niño expectantly causes warmer SAT anomalies over the central equatorial Pacific Ocean bounded by cooling on both sides. The atmospheric cooling encompasses the islands of the tropical western Pacific as well as affecting western and southern Australia. Eastern India, Eastern Europe, and the subtropical east coast of South America experience cooler temperatures.

1.3 Motivation and hypothesis

Recent research suggests EP and CP statistics have been changing over the past few decades. Using ERSSTv2 (Smith and Reynolds, 2004), Kao and Yu (2009) stated that CP El Niño occurs more frequently in recent decades. Lee and McPhaden (2010) analyzed high-resolution satellite AVHRR SST data and found an increase in CP El Niño frequency and intensity from 1982-2010. Yu et al. (2012) investigated CP and EP events in the ERSSTv3b (Smith and Reynolds 2004) observational SST data over the time period of 1950-2010 and also discovered an increase in CP El Niño frequency.

Research by Deser et al. (2010) found that different SST data sets used in climate analysis showed inconsistencies in the representation of long term trends in the central Pacific. The authors showed that Kaplanv2 and HadISST1 both demonstrated a cooling trend in the Niño 3.4 region, while ERSSTv3b, and un-interpolated ICOADS and HadSST2 data showed significant warming in the eastern equatorial region of the Pacific. Using marine cloudiness, precipitation, and SLP data, the authors argued that the data showing a warming trend were more physically consistent with the atmospheric data over

the twentieth century. The authors argued that the cooling trend must be a result of the methodology used in interpolating and reconstructing these simulated data sets.

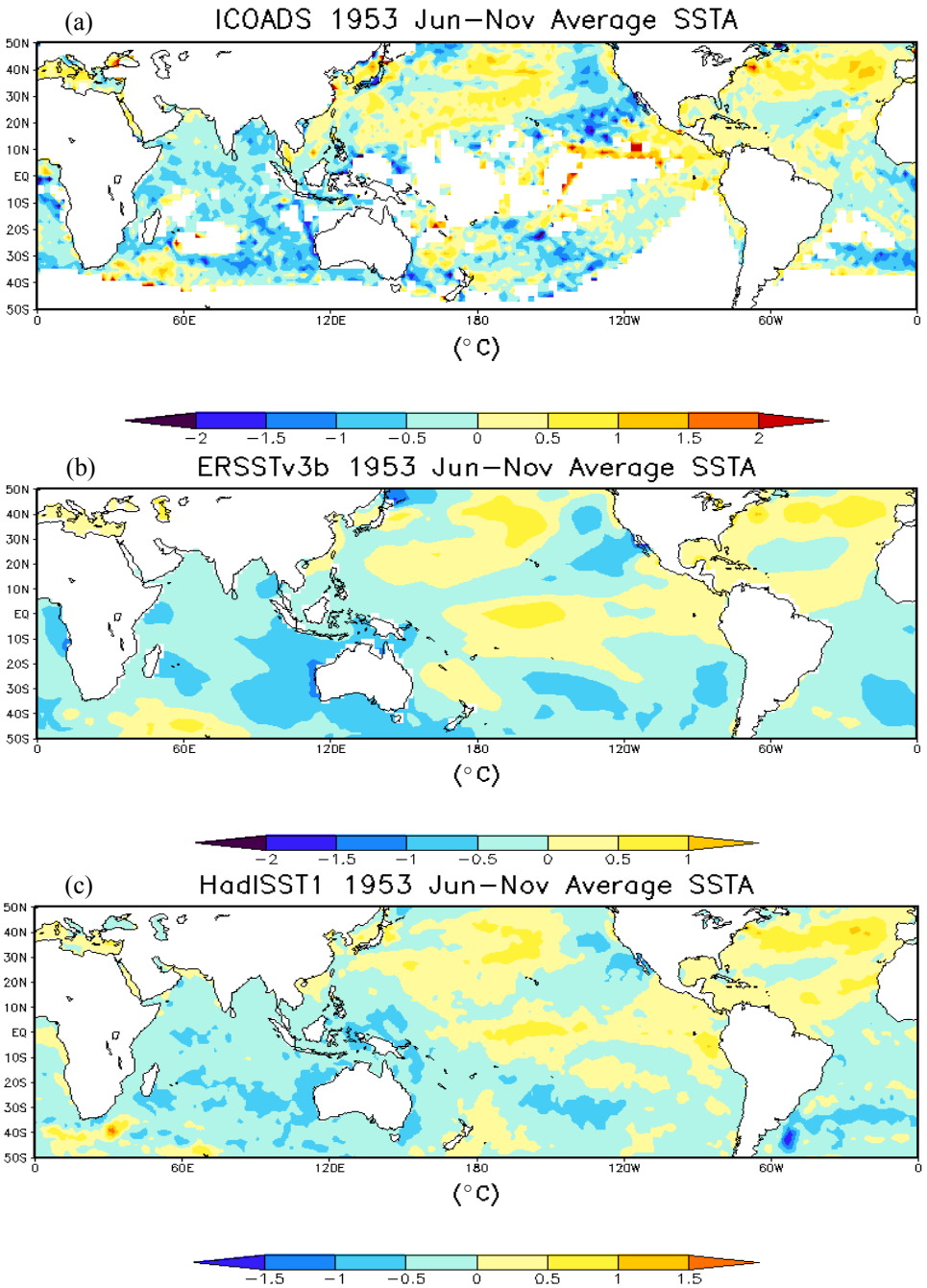

Figure 6. (a) ICOADS 1953 Jun-Nov Average SSTA. (b) ERSSTv3b 1953 Jun-Nov Average SSTA. (c) HadISST1 1953 Jun-Nov Average SSTA.

When identifying and classifying CP and EP El Niño events, the discrepancy between the datasets is equally important because of the paucity of data in the central Pacific in the earlier historical record. Figure 6 shows the six month average SSTA during the development of the 1953-54 CP event (Yu et al., 2012). The largest anomalies in the ICOADS data are found in the east Pacific, and there is a considerable area in the central Pacific devoid of data. In the ERSSTv3b there is clearly a stronger CP signal than the ICOADS figure and a weaker signal in the Niño 1+2 region (used in three of the four metrics used to define a CP El Niño) than that in the HadISST1 case. It is evident that the classification of this event is highly dependent not only on the particular methodology used in the data interpolation but also on the particular metric used in the classification of CP and EP events. The discrepancies among the differing datasets become less significant after the late 1970s when more comprehensive coverage was made possible by satellite observations. It seems justifiable then, to suggest that recent studies citing changes in the statistics of ENSO over the past several decades are influenced by changes in data quality.

I propose the following hypothesis:

The statistics of CP and EP El Niño events have not changed significantly over the past half-century.

To test this hypothesis I employ a two-part data analysis procedure.

1) Examine the consistency of the classification of CP and EP El Niño events since 1950 using multiple datasets and multiple metrics drawn from the peer reviewed literature.

2) Test the significance of the recent changes in CP and EP El Niño statistics with the incorporation of spatially and temporally complete and consistent coupled model output from state of the art coupled climate models.

CHAPTER 2

DATA

2.1 Observational Data

To examine the consistency of CP and EP El Niño event classification in differing observational estimates of sea surface temperature, I incorporate five data sets used in the peer reviewed literature to study historical changes in tropical Pacific SST. The datasets are listed in Table 1.

Table 1. Observational SST Data used. All analysis data is referenced from other work.

Data Name	Type	Reference	Spatial Resolution
International Comprehensive Atmosphere-Ocean Data Set (ICOADS)	Raw	None	2°x2°
Hadley Centre SST version 2 (HadSST2)	Un-Interpolated based on ICOADS	(Rayner et al., 2006; Minobe and Maeda, 2005)	2°x2°
Hadley Centre sea ice and SST version 1 (HadISST1)	Re-Analysis (Interpolated)	(Rayner et al., 2003)	1°x1°
Extended Reconstructed SST version 3 (ERSSTv3b)	Re-Analysis (Interpolated)	(Smith et al., 2008)	2°x2°
Kaplan Extended SST version 2 (Kaplanv2)	Re-Analysis (Interpolated)	(Kaplan et al., 1998)	5°x5°

The ICOADS data set is a digital database that was constructed in 1985 and continues to be updated. It contains raw data recorded by ships, weather ships, and weather buoys dating back to 1800. The HadSST2 data set is the work of Rayner et al. (2006) and is an observational dataset based on the ICOADS SST data set. The HadSST2 analyzed the ICOADS SST database and did bias corrections to account for measurement practices through time. A detailed analysis of uncertainties in these

corrections was included as well as an assessment of total uncertainty in each gridded average. The analysis was done by combining the bias-correction-related uncertainties with those arising from measurement errors and under-sampling of intragrid box variability. No interpolation was done in this SST data set that spans from 1850-present.

Each re-analysis data set was created using methods that differ from the next. In Kaplan et al. (1998) SST anomalies were produced using four statistical methods; optimal smoothing (OS), the Kalman filter (KF), optimal interpolation (OI), and Projection Method (P). These Empirical Orthogonal Functions (EOFs) are sourced by the stationary spatial covariance of the data field and use this covariance as the key to filling in missing data from 1856-1991. The Kaplanv2 data set consists of the Global Ocean Surface Temperature Atlas (GOSTA) monthly averages of individual SST observations for 5° latitude by 5° longitude boxes (Bottomley et al., 1990) as the observational data. The MOHSST5 data set, which incorporates ICOADS, is used where no GOSTA data existed. It should be noted that MOHSST5 corrects for systematic biases in SST measurements. Climatological monthly means for the period 1951-1980 are subtracted out leaving the analysis product (Kaplanv2) as an anomaly from this mean. The Kaplanv2 data set spans from 1856 to present.

The HadISST1 data set is a product of Rayner et al. (2003) where a suite of methods was used to create a spatially complete monthly SST analysis from 1871-present. The HadISST1 data set was developed at Met Office Hadley Centre for Climate Prediction and Research, and improved on previous SST and sea ice data sets: GISST1, GISST2, and GISST3; all developed at Hadley Centre. From 1871-1981 all SST analysis used gridded, quality-controlled in situ SST observations. From 1871-1941 the data were

bias-adjusted following Folland and Parker (1995) because of diverse methods of data retrieval with different biases. In addition, for the data-sparse oceanic regions a reduced space optimal interpolation (RSOI) (Kaplan et al., 1997) was utilized to fill in these regions using a 4° area resolution from 1871-1948 and a 2° area resolution from then to 1981. The RSOI uses EOFs to reconstruct in-situ data based on ships' observations and in later years remotely sensed SSTs. From 1982 onward, the RSOI technique was applied to a combination of in situ/satellite SSTs. The bias-adjusted non-interpolated gridded in situ data were then adjusted and blended with the reconstructed fields. The HadISST1 field is a blend of EOF reconstructed data with original data (Rayner et al., 2003).

The ERSSTv3b data set is a product of another re-analyses conducted by Smith et al. (2008). The output being simulated surface temperature data (LST and SST) that is a combination of model output and observed data along with the 5°x5° historical sampling grid from 1880-present. The model output comes from the Geophysical Fluid Dynamics Laboratory (GFDL) Climate Model 2.1 (CM2.1), which is a coupled general circulation model (CGCM) that simulates the large-scale climate signal using variations in forcing by greenhouse gases, aerosols, and estimates of solar radiation changes. Low frequency anomalies from 1860-2000 are combined with high frequency variations done with OI to make for a realistic data field. The simulated data were subsampled using the historical sampling grid with random errors added in to produce test temperature-anomaly reconstructions, that are validated against the full (error free) simulated data. Low frequency and High frequency tuning was then done in order to improve the original simulated data. In-situ ship and buoy SSTs are taken along with bias-adjusted satellite

SSTs in later years and are combined to form the merged data set that is used in the statistical analysis. Using weights calculated using relative noise of the data types and normalization of these weights ensure no damping or inflation is present in the data. The ERSSTv3b data set spans the time period 1854 to present.

2.2 Model Data

Model data comes from the fifth phase of the Coupled Model Intercomparison Project (CMIP5) established by the Working Group on Coupled Modeling under the World Climate Research Program. The simulations come form the pre-industrial control (Pi-control) simulations, which serve as a baseline for the analysis of historical and future scenario simulations. The Pi-control simulations are run with prescribed concentrations of well-mixed greenhouse gases that allow for estimation of unforced variability in the coupled model. Here, simulated SST output is analyzed from 16 CMIP5 member models.

The choice of Pi-control CMIP5 data for the Monte Carlo simulation allows for a longer record of physically consistent and comprehensive data. Unlike the observational data, the CMIP5 output has no gaps in coverage and is not affected by changing concentrations of greenhouse gasses. In this way, the model output can be seen as a "perfectly sampled" version of nature. Of course, the statistics of natural climate phenomena such as ENSO can vary considerably among coupled models and from the observed phenomena. Because of this an analysis of ENSO statistics was undertaken to identify models with similar statistics to those of the observed phenomenon.

CHAPTER 3

METHODS

3.1 EP and CP El Niño Metrics

There is no consensus to date in the literature for a metric to classify a CP El Niño. Trenberth and Stepniak (2001) argued that to properly characterize the different flavors of El Niño, more than one index must be used. Here, we incorporate the TNI of Trenberth and Stepaniak (2001) as well as three other indices that were recently reviewed by Yu et al. (2012) to determine the "flavor" of El Niño events from 1950-2010. All data had to first pass the working definition for an El Niño before the metric was applied. The four metrics are described below:

1. The Niño 3/4 Index: (Yeh et al., 2009, Lee and McPhaden., 2010)

CP: (SSTA) Niño 4 > Niño 3 and >= 0.5°C for December-January-February (DJF)
EP: (SSTA) Niño 3 > Niño 4 and >= 0.5°C for December-January-February (DJF)

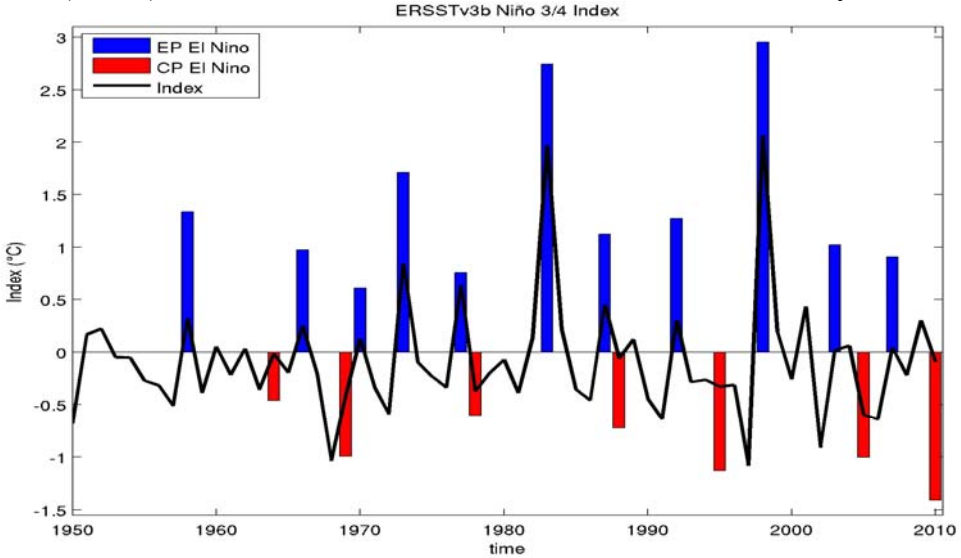

Figure 7. ERSSTv3b Niño 3/4 Index. The Niño 3/4 index applied to ERSSTv3b from 1950-2010. The EP index associated with EP El Niño events are displayed in blue. The CP index associated with CP El Niño events are displayed in red. All values are displayed in °C.

The Niño 3/4 index is defined as the Niño 3 SSTA – Niño 4 SSTA. When applied to an El Niño event, if the Niño 3/4 index > 0 then an EP El Niño is present. If the Niño 3/4 index < 0 a CP El Niño is present.

2. The EP/CP Index: (Kao and Yu, 2009)

CP: SSTAs confined to Niño 3.4 and Niño 4 regions
EP: SSTAs mostly contained to Niño 1+2 and Niño 3 regions

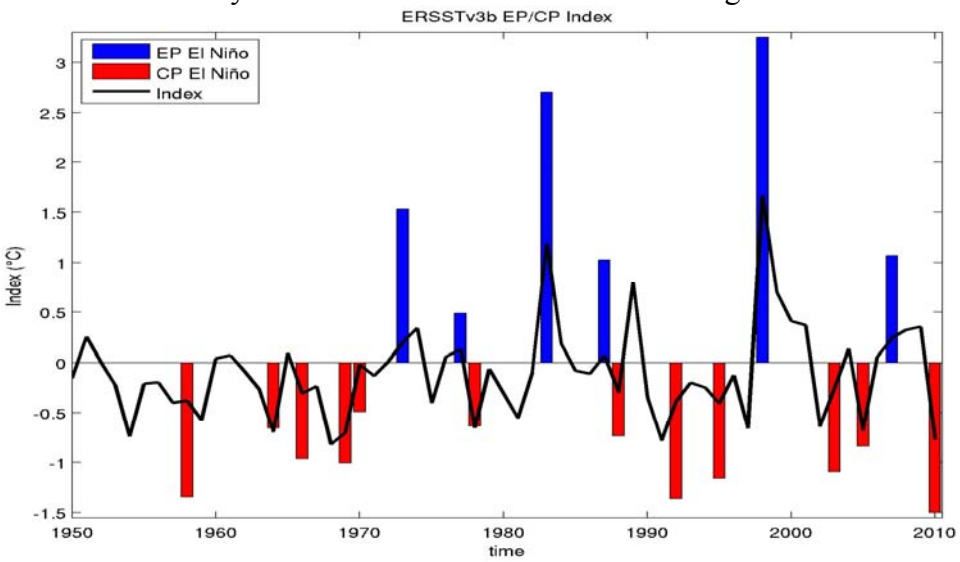

Figure 8. ERSSTv3b EP/CP Index. The EP/CP index applied to ERSSTv3b from 1950-2010. The EP index associated with EP El Niño events are displayed in blue. The CP index associated with CP El Niño events are displayed in red. All values are displayed in °C.

The EP/CP Index is defined here as the average Niño (1+2 and 3) SSTA – average Niño (3.4 and 4) SSTA. When applied to an El Niño event, if the EP/CP index > 0 then an EP El Niño is present. If the Niño 3/4 index < 0 a CP El Niño is present. Kao and Yu (2009) attempted to isolate the CP (EP) signals by removing (via linear least squares regression) the Niño 1+2 (Niño3.4) index from the data and performing Empirical Orthogonal Function analysis on the residuals. Here we reproduce their results using a more straightforward index based approach.

3. The El Niño Modoki Index (EMI): (Ashok et al., 2007)

$EMI = [SSTA]_A - 0.5*[SSTA]_B - 0.5*[SSTA]_C$
Region A (165°E–140°W, 10°S–10°N), B (110°W–70°W, 15°S–5°N), and C (125°E–145°E, 10°S–20°N)

CP: EMI > 0.7σ average over Winter Seasons
EP: EMI < 0.7σ average over Winter Seasons

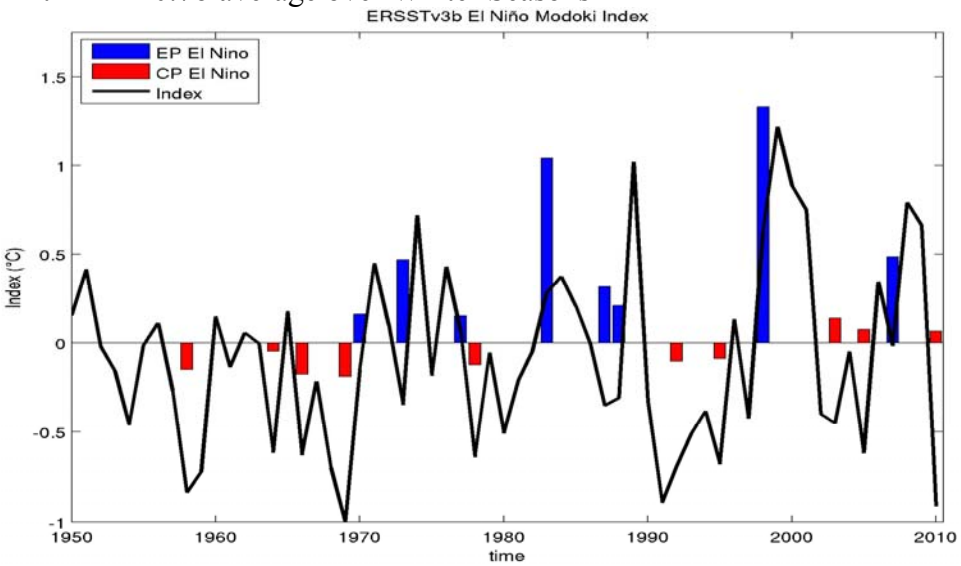

Figure 9. ERSSTv3b El Niño Modoki Index. The El Niño Modoki index applied to ERSSTv3b from 1950-2010. The 0.5*Region B metric associated with EP El Niño events are displayed in blue. The 0.5*Region C metric associated with CP El Niño events are displayed in red. All values are displayed in °C.

The EMI is defined as the Region A SSTA – 0.5*Region B SSTA – 0.5*Region C SSTA. Here, the EMI is multiplied by negative 1 in order to compare with the other metrics. When applied to an El Niño event, if the EMI >0.7σ then an El Niño Modoki (CP El Niño) is present. If this threshold remains unbroken, then the El Niño event is simply classified as an EP El Niño.

4. The Trans Niño Index (TNI): (Trenberth and Stepaniak, 2001)

CP: Niño $1+2_N$ – Niño 4_N = some negative value
EP: Niño $1+2_N$ – Niño 4_N = some positive value
(Niño $1+2_N$ = Niño 1+2 SSTA/Niño 1+2 σ, Niño 4_N = Niño 4 SSTA/ Niño 4 σ)

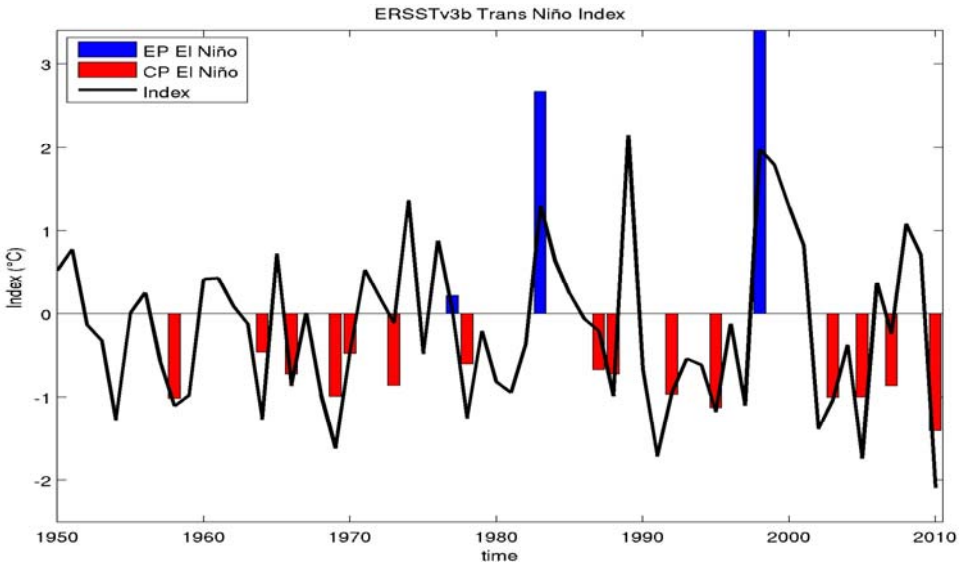

Figure 10. ERSSTv3b Trans Niño Index. The Trans Niño index applied to ERSSTv3b from 1950-2010. The EP index associated with EP El Niño events are displayed in blue. The CP index associated with CP El Niño events are displayed in red. All values are displayed in °C.

The TNI is defined as the Niño $1+2_N$ SSTA – Niño 4_N SSTA. When applied to an El Niño event, if the TNI > 0 then an EP El Niño is present. If the TNI < 0 a CP El Niño is present

3.2 Monte Carlo Simulation

Resampling is a category of statistical methods that is used to robustly test a sample population. Results commonly take the form of sample means, variances, standard errors, and confidence intervals. Some popular resampling techniques are the Bootstrap, Jack knife, or Monte Carlo test. In a Monte Carlo test, a small (relative to population size) random sample is taken. The small sample is taken randomly from the population any number of times before being synthesized into a new sample population, which can be used to accept or reject a null hypothesis about the original sample. Here,

the significance of the Lee and McPhaden (2010) results is tested using a Monte Carlo test.

Lee and McPhaden (2010) applied the Niño 3/4 Index to High Resolution AVHHR OI daily SST data for the December-January-February (DJF) season from 1982-2010 and found an increase in CP El Niño frequency and intensity. I utilize Monte Carlo simulations that incorporate CMIP5 model output to test whether the 28-year trends described by Lee and McPhaden (2010) are statistically significant when sampled over the longer "perfectly sampled" period of the CMIP5 simulations.

The methods used by Lee and McPhaden (2010) are tested on SST output from 16 Pi-control simulations. The Monte Carlo simulations include 1000 random samples (with replacement) of 28 year "chunks" of data from the record. For each 28-year sample, the December-January-February (DJF) seasonally averaged Niño 3 and Niño 4 SSTAs are calculated (representing the mature phase of El Niño) and compared to assess the CP to EP frequency in the sample. Next, linear trends are calculated for the Niño regions over the 28-year sample. Note, only samples that meet the NOAA threshold for an El Niño (0.5 °C, or standard deviation equivalent) are considered in the trend. Results represent the distribution of trends in the "perfectly sampled" observations of the individual models and multi model means and provide a context with which to consider the claims of Lee and McPhaden (2010).

CHAPTER 4

RESULTS AND DISCUSSION

4.1 Observational Data Analysis

In this section I examine metrics used in the literature to distinguish CP and EP events using several observational estimates of historical SST records. Table 2 shows the El Niño events occurring since 1950 and the classification of the event for each of the metrics described in Section 3. The Observational SST data sets are examined using four CP/EP El Niño metrics to classify El Niño events for the time period of 1950-2010. The analysis reveals several inconsistencies among the four metrics used to identify CP and EP events in the observational record. Table 2 documents a total of 18 El Niño events (as opposed to the 21 synthesized by Yu et al.; 2012). Of the 18 El Niño events shown above, the 4 metrics are in total agreement on the "flavor" of El Niño for 9 events. The other half of the El Niño events reveal varied disagreement among the metrics used in distinguishing the type of the El Niño present.

Table 2. Using ERSSTv3b the Results of Yu et al. (2012) are re-created. Years highlighted in red denote a disagreement between Yu et al. (2012) result and the result of this analysis. Yu et al. (2012) used ERSSTv3b in their analysis, but applied a 30 –year running climatology. Here a fixed 30-year climatology (1971-2000) is used. All events were checked using the NOAA criteria for an El Niño event.

El Niño Years	Niño 3/4 Index:	EP/CP Index:	EMI:	TNI:	Raw Data Coverage %	
1951-52					Niño 3: 31%	Niño 4: 22%
	Neutral	Neutral	Neutral	Neutral		
1953-54					26%	14%
	Neutral	Neutral	Neutral	Neutral		
1957-58					50%	25%
	EP	CP	CP	CP		
1958-59					39%	28%
	Neutral	Neutral	Neutral	Neutral		
1963-64					70%	56%
	CP	CP	CP	CP		
1965-66					80%	60%
	EP	CP	CP	CP		
1968-69					65%	56%
	CP	CP	CP	CP		
1969-70					82%	56%
	EP	CP	EP	CP		
1972-73					64%	66%
	EP	EP	EP	CP		
1976-77					86%	65%
	EP	EP	EP	EP		
1977-78					78%	75%
	CP	CP	CP	CP		
1982-83					FULL	COVERAGE
	EP	EP	EP	EP		
1986-87					FULL	COVERAGE
	EP	EP	EP	CP		
1987-88					FULL	COVERAGE
	CP	CP	EP	CP		
1991-92					FULL	COVERAGE
	EP	CP	CP	CP		
1994-95					FULL	COVERAGE
	CP	CP	CP	CP		
1997-98					FULL	COVERAGE
	EP	EP	EP	EP		
2002-03					FULL	COVERAGE
	EP	CP	CP	CP		
2004-05					FULL	COVERAGE
	CP	CP	CP	CP		
2006-07					FULL	COVERAGE
	EP	EP	EP	CP		
2009-10					FULL	COVERAGE
	CP	CP	CP	CP		

The discrepancy regarding the "flavor" of the El Niño event present during the period of 1950-2010 is even more pronounced once the metrics are applied to multiple data sets. Figure 11 shows the number of EP and CP events for the 5 observational SST data sets using the 4 different metrics over the time period: 1950-2010. Table 3 reveals useful statistics for interpreting the results in Figure 11. Note that Kaplanv2 contains SST anomalies computed using a 1951-1980 seasonal climatology. This is inconsistent with the climatology (1971-2000) used in the studies of interest here.

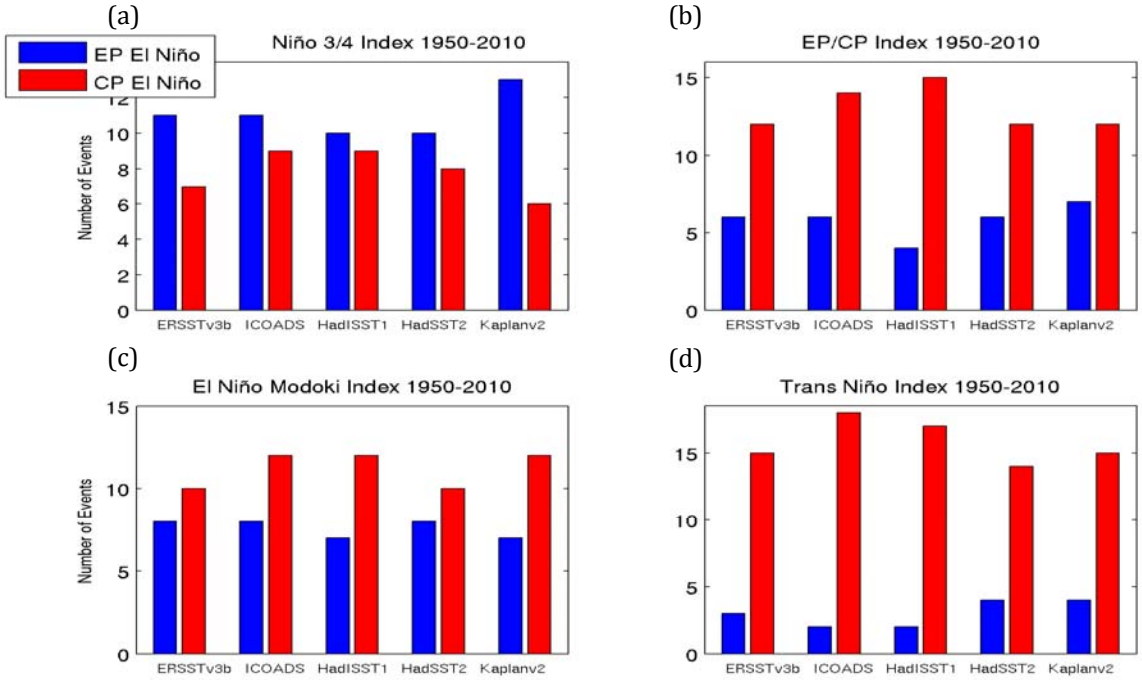

Figure 11. Number of EP and CP types of El Niño from 1950-2010 for Observational Data Sets: ERSSTv3b, ICOADS, HadISST1, HadSST2, Kaplanv2. (a) Niño 3/4 Index 1950-2010 (b) EP/CP Index 1950-2010 (c) El Niño Modoki Index 1950-2010 (d) Trans Niño Index 1950-2010.

Table 3. Statistics of Observational SST data sets once four different metrics are applied in order to determine the "flavor" of El Niño.

Metric:	Data Set:	# of Events (1950-2010)		EP index:	CP Index:
		EP	CP	Variance (°C)	Variance (°C)
Niño 3/4 Index					
	ERSSTv3b	11	7	0.733	0.375
	ICOADS	11	9	0.724	0.432
	HadISST	10	9	0.693	0.361
	HadSST2	10	8	0.770	0.475
	KAPLAN	13	6	0.689	0.387
EP/CP Index					
	ERSSTv3b	6	12	0.837	0.498
	ICOADS	6	14	0.842	0.509
	HadISST	4	15	0.763	0.463
	HadSST2	6	12	0.891	0.526
	KAPLAN	7	12	0.769	0.482
El Niño Modoki Index					
	ERSSTv3b	8	10	0.142	0.020
	ICOADS	8	12	0.144	0.023
	HadISST	7	12	0.130	0.020
	HadSST2	8	10	0.156	0.023
	KAPLAN	7	12	0.136	0.017
Trans Niño Index					
	ERSSTv3b	3	15	1	1
	ICOADS	2	18	1	1
	HadISST	2	17	1	1
	HadSST2	4	14	1	1
	KAPLAN	4	15	1	1

The Niño 3/4 Index uses two regions of comparable variance and spatial area as indices. An EP El Niño identifies strongest SSTAs in the Niño 3 region, while strongest anomalies are focused in the Niño 4 region during a CP El Niño. In using this straightforward approach, The Niño 3/4 Method yields results that may only be skewed by the slightly larger variance in the Niño 3 region. It is the only index that consistently classifies a larger number of EP events to CP events with the largest difference found in the Kaplan data.

The EP/CP Index describes a CP El Niño as having SSTAs confined to the Niño 3.4 and 4 regions, and an EP El Niño as having SSTAs mostly contained to Niño 1+2 and Niño3 regions. The regions used to define EP and CP indices have a large spatial coverage and comparable variability differences seen in the NINO3/4 index. While the large area does a good job of qualitatively explaining the spatial nature of these two types of El Niño, the nature of the index calculation and climatological range of temperature values averaged in these area averages leads toward the dominance of CP El Niño in the results.

The El Niño Modoki Index uses meridionally large regions that are separate from the popular Niño regions. These area averages are used to calculate an index that must break a 0.7σ threshold in order for the event to be termed an El Niño Modoki (CP El Niño). If this threshold isn't broken, but the Niño 3.4 index is greater than or equal to 0.5 °C for the necessary period of time, then it is termed an (EP) El Niño. The use of a standard deviation (σ) tends to favor El Niño Modoki (CP El Niño) slightly. Note the EP index is an order of magnitude greater than the CP.

The Trans Niño Index uses normalized area averaged SSTAs. The Niño 1+2 (large variance) and Niño 4 (moderate variance) regions are first divided by their standard deviation before calculating the index. This metric was first created in order to define the "tilt" of the El Niño event (Trenberth and Stepaniak, 2001). When applied here as a way of defining the "flavor" of the El Niño event, this metric leans heavily toward the CP type of El Niño. A strong argument for this is the choice of the Niño 1+2 region as the EP El Niño index. As displayed in the Niño 3/4 Method, the Niño 3 region defines this index more reliability. The Niño 1+2 region is also smaller than the Niño 4

region; therefore using much less data to define an event (EP El Niño) that at times has warm anomalies covering two thirds of the entire Equatorial Pacific Ocean.

4.2 Monte Carlo Analysis

Following the methodology of Lee and McPhaden (2010), I applied Monte Carlo simulations to SST output from 16 coupled climate models of the CMIP5 project. Using the statistics of CP and EP El Niño frequency and Niño region variances from observations, I first selected the SST output from the NSF-FASTCHEM coupled model as a statistically similar representation of the observed CP EP statistics. Figure 12 shows the distribution of the ratio of CP El Niño to the total number of El Niño events (CP+EP) in the NSF FASTCHEM model. The mean value of 0.55 found in the observational analysis (indicated by the red box), is within one standard deviation of the simulated frequency of occurrence in the model. A list of all of the CMIP5 coupled models with the calculated CP frequencies and Niño region variances are listed in Table 4.

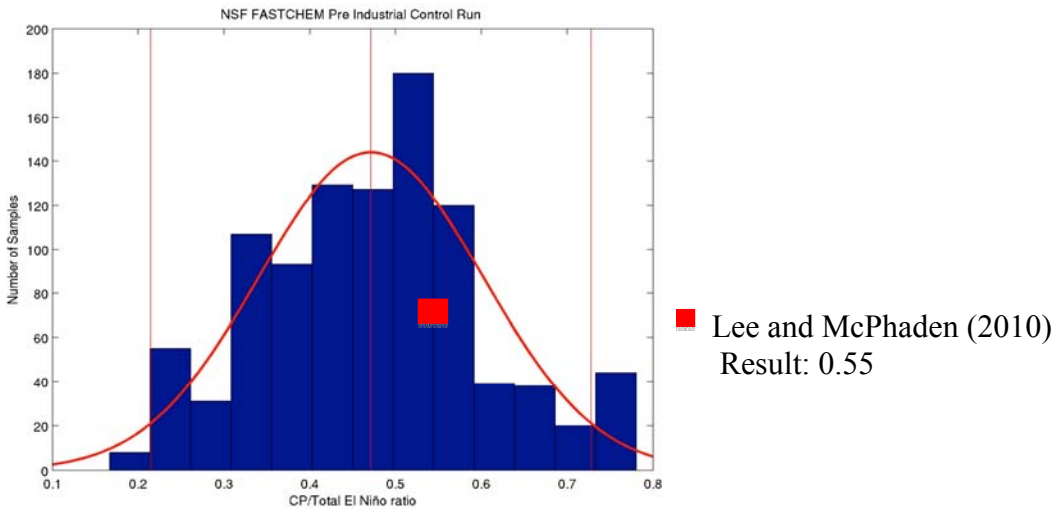

Figure 12. NSF FASTCHEM Pre Industrial Control Run. The distribution of CP El Niño frequency in NSF FASTCHEM resulting from the Monte Carlo Simulation is demonstrated. The middle red line denotes the sample mean with either red line outside of it showing the 95% confidence interval.

Table 4. Statistics from pre industrial runs using 16 different model outputs found in the latest CMIP5.

Model Name	(#)	CP/Total Ratio	Variance: (°C)		
			Niño 3	Niño 4	Niño 3.4
AVHRR OI SST (1982-2010)		0.55	0.7808	0.4292	0.7515
ERSSTv3b (1950-2010)		0.40	0.8114	0.3924	0.7403
Multimodel Mean		0.402 ±0.183	0.883	0.604	0.963
CMCC-CMS	1	0.4579±0.17	0.6413	0.5415	0.8748
CSIRO-0	2	0.0712±0.07	0.9022	0.3206	0.7277
CSIRO-3	3	0.255±0.20	0.6737	0.4071	0.5974
INM	4	0.468±0.61	0.2742	0.2175	0.323
IPSL-CM5A-LR	5	0.204±0.21	0.4306	0.338	0.4408
IPSL-CM5A-MR	6	0.519±0.21	0.51	0.55	0.585
IPSL-CM5B-LR	7	0.077±0.08	0.57	0.21	0.556
MPI-M-LR	8	0.528±0.19	0.65	0.55	0.719
MPI-M-P	9	0.734±0.18	0.64	0.55	0.71
MRI-CGCM3	10	0.546±0.16	0.37	0.3476	0.4128
NCAR-CCSM4	11	0.438±0.15	1.30	0.966	1.569
NCC-M	12	0.198±0.11	1.081	0.522	0.948
NSF-BGC	13	0.387±0.19	1.298	0.894	1.538
NSF-CAM5	14	0.698±0.14	0.938	1.015	1.219
NSF-FASTCHEM	15	0.4594±0.132	1.241	0.846	1.4693
NSF-WACCM	16	0.397±0.13	2.6109	1.3814	2.7199

Figure 13 shows the distribution of linear SST anomaly trends for El Niño events in the Niño 3 and 4 regions of NSF FASTCHEM SST from the Monte Carlo Simulation. Lee and McPhaden (2010) pointed to an increase in CP El Niño intensity manifesting a positively trending Niño 4 SST anomaly (0.20 °C/decade), countered by a "decrease" in EP El Niño intensity exhibited in a negative trend in the Niño 3 SST anomaly (-0.39 °C/decade), though the trend was not significant by their own analysis. All results from Lee and McPhaden (2010) lie within the 95% confidence interval (CI) (1.96σ) of the NSF FASTCHEM pi-control mode.

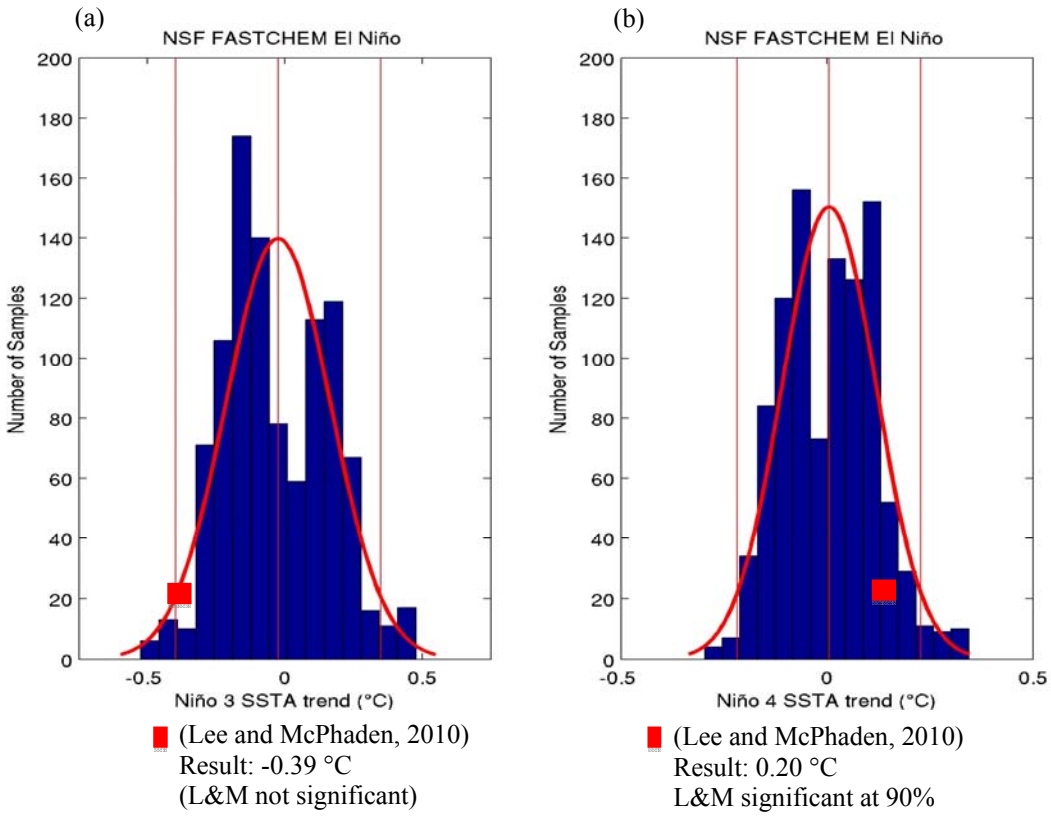

Figure 13. (a) NSF FASTCHEM El Niño (b) NSF FASTCHEM El Niño. The distribution of NSF FASTCHEM Decadal SSTA trends (°C) resulting from the Monte Carlo Simulation is demonstrated. The middle red line denotes the sample mean with either red line outside of it showing the 95% CI. The red box refers to the result of Lee and McPhaden (2010).

Figure 14a-b shows the results of the Monte Carlo simulation applied to output from 13 members (CSIRO-0, IPSL-CM5B-LR, and NCC-M were omitted for CP/Total ratios below the 1.96σ threshold) of the CMIP5 coupled model project. The multi model averages place the results of Lee and McPhaden (2010) into a broader representation of "perfectly sampled nature" where the frequency of occurrence and ENSO behavior vary significantly. The frequency of occurrence of CP El Niño found in the observational data lies within the one standard deviation of 9 out of the 13 models used in this analysis. This multi model mean demonstrates a CP/Total El Niño ratio that contains the Lee and

McPhaden (2010) result within its first standard deviation with slightly larger variance in the Niño 3 and 4 regions (see Table 4).

(a)

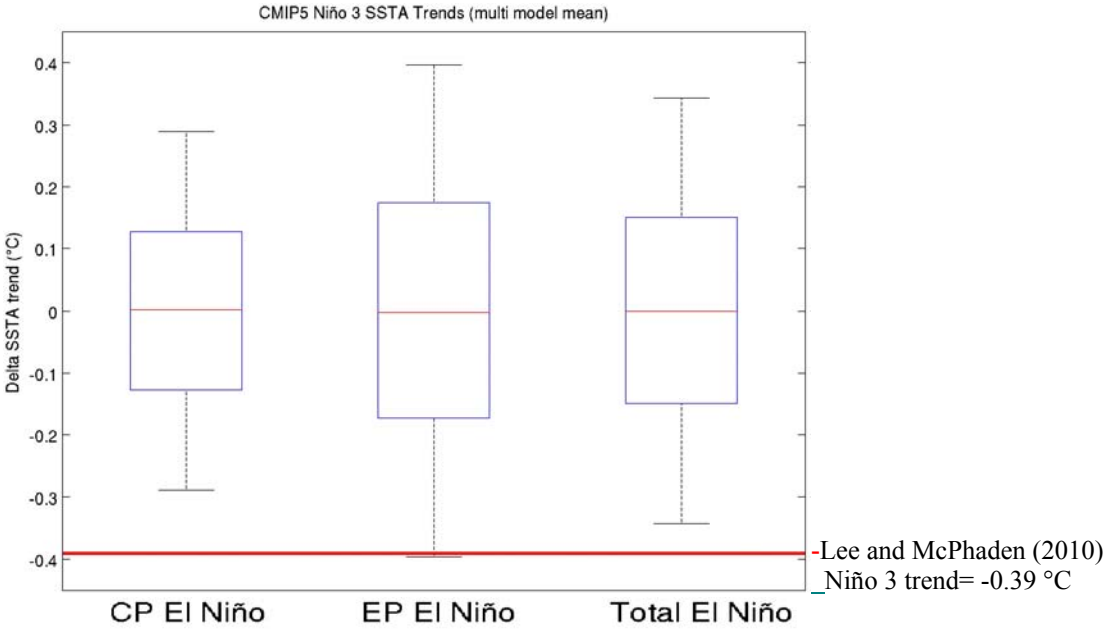

(b)

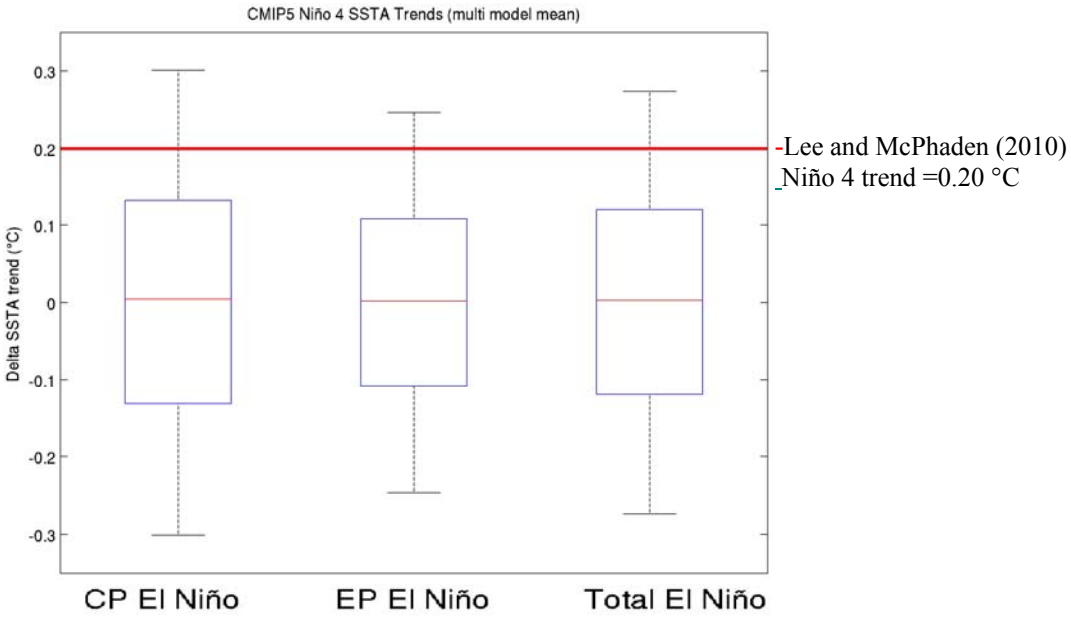

Figure 14. (a) CMIP5 Niño 3 SSTA Trends (multi model mean) (b) CMIP5 Niño 4 SSTA Trends (multi model mean). Distributions of Multimodel Mean Decadal SSTA trends for CMIP5 piControl runs for (a.) EP Niño 3, CP Niño 3, and Niño 3 average (b.) EP Niño 4, CP Niño 4, and Niño 4 average. The trend result for Lee and McPhaden (2010) is plotted on the Niño 3 and 4 figures to compare with model results.

Each Figure is described as such: Red lines denote the mean surrounded by a blue box signifying the 1st quartile, with arms extending to 1.96 σ or a 95% CI. Multimodel means were calculated with the omission of models: CSIRO-0, IPSL-CM5B-LR, and NCC-M, because of their statistical disagreements displayed in Table 4. SST anomaly trends are in the form of °C/decade.

Figure 14 shows the distribution of the multi model averaged SST anomaly trends for CP and EP El Niño over the Niño 3 and Niño 4 regions. All calendar months that meet the NOAA criteria of for an El Niño event are used in the trend analysis. Figure 14a shows the distribution of the Niño 3 linear trends for CP, EP, and total El Niño (CP+EP) events. The -0.39°C/decade trend of Lee and McPhaden (2010) falls just within the 95% CI for EP events and outside the 95% CI for CP and total El Niño events. Figure 14b shows the multi model average distribution of the Niño 4 linear trends for CP, EP, and total El Niño (CP+EP) events. The 0.20°C /decade trend of Lee and McPhaden (2010) falls well within the 95% CI for CP, EP, and total events. The results suggest that the increasing intensity of Niño 4 SSTA observed by Lee and McPhaden (2010) over the past 28 years is unlikely to be significant when considered over longer timescales in the context of comprehensive, physically consistent data. Recall, the declining trend in the Niño 3 SSTA was not statistically significant in the Lee and McPhaden analysis. Here is well outside the 95% CI for CP El Niño and this is also seen in the combined (CP+EP) case. Results of the Monte Carlo simulation for each model are shown in Figure A1 (Appendix).

Naturally forced model output is not the same as observational data, but it can help to understand the behavior of the system in question, which in this case is the variability of El Niño. The fact that both the "increasing" decadal SSTA trend in the Niño 4 region as well as the "decreasing" decadal SST trend in the Niño 3 region fall

within the 95% CI in the model that best simulates the observed tropical Pacific SSTs suggests that the 28 year period used by Lee and McPhaden (2010) was too short for the results presented.

CHAPTER 5

CONCLUSIONS

This analysis aims to address the question of an increase in CP El Niño intensity over the past thirty years. The observational data analysis serves to assess the consistency of the metrics used to measure CP and EP events and to test the impacts of differing interpolation techniques used in the creation of historical SST datasets. Consistent with my hypothesis, Table 2 shows that the strongest discrepancy lies before full data coverage was available by satellites in 1979. Years preceding 1950 were omitted because of the increasing sparseness of raw, un-interpolated data in the equatorial Pacific. The interpolation methods used by ERSSTv3b, HadISST1, and Kaplanv2 are unique to each data set, and when applied to raw SST data with pronounced gaps in coverage the Central Pacific they produced varied results (Figure 6). The before-mentioned disagreement is even more pronounced when aiming to define the flavor of El Niño. Each metric used in this study takes a different approach to defining an EP or CP El Niño. These approaches combined with the present discrepancy among observational data sets yielded diverse results. For the 1950-2010 time period, the number of total ENSO events remained fairly consistent across all of the data (between 18 and 20); however the number of defined CP and EP El Niño events fluctuated. As mentioned previously, the results from the Niño 3/4 Index yielded the most consistent results over all data sets with an average of 11 EP and 7.8 CP El Niño events during the time period in question. The comparison between the Niño 3 and 4 regions takes area averaged SSTAs from two "blocks" of similar spatial area (Niño 3: 5°S-5°N, 150°W-90°W; Niño 4: 5°S-5°N, 160°E-150°W) and of comparable variance (1982-2010: Niño 3: 0.788; Niño

4: 0.404). The El Niño Modoki Index also gave balanced results with an average of 7.6 EP and 11.2 CP El Niño events present. The EP/CP Index and Trans Niño Index leaned heavily toward CP El Niño. The EP/CP Index returned an average CP:EP ratio of 2.24:1 and the TNI yielded an average ratio of 5.27:1. This tendency to favor the CP type of El Niño puts the validity of these two metrics in question with regards to this specific use of each.

The Monte Carlo Analysis applied to 16 CMIP5 Pi-control models provides a substantial number of data points that can be tested for significance. In the model analysis, the results of CP El Niño frequency demonstrated that the result of Lee and McPhaden (2010) lies within the first standard deviation of the multi model mean calculated with the omission of models: CSIRO-0, IPSL-CM5B-LR, and NCC-M. The multi model mean result describes the "increase" in CP El Niño frequency that is well within the natural variation of ENSO. The Monte Carlo Analysis result for CP El Niño intensity demonstrates that the result of Lee and McPhaden (2010) lies within the 95% CI of the multi model mean SSTA trend. Therefore expressing the "increase" in CP El Niño intensity as well within the natural variation of ENSO. The analysis of the Niño 3 SSTA trend suggested, as the -0.39 °C/decade SSTA trend found by Lee and McPhaden (2010) fell within 1.96σ (95% CI) of El Niño events in the NSF FASTCHEM model, but outside the 95% CI for the multi model mean. The Lee and McPhaden (2010) Niño 3 SSTA trend was found to be not significant by their own standards.

In summary, the classification of differing types of El Niño is limited by the lack of consistent and standardized metrics. Further, the choice of data used to understand the changing statistics of El Niño events can have a significant impact on results. By

incorporating comprehensive model output from state of the art coupled climate simulations and resampling techniques, I provide evidence that the changes observed in CP El Niño intensity over the past three decades, manifesting itself in a positively trending Niño 4 SSTA, falls well within the expected range of values and thus I cannot reject my hypothesis. As full data coverage continues in the future and a larger comprehensive observational data set presents itself, the variation of CP and EP El Niño will become clearer, thus providing the means for a more definitive conclusion on the current state of the tropical Pacific Ocean.

REFERENCES

Ashok, K., S. K. Behera, S. A. Rao, H. Weng, and T. Yamagata (2007), El Niño Modoki and its possible teleconnection, *J. Geophys. Res., 112*, C11007, doi:10.1029/2006JC003798.

Bjerknes, J. (1969), Atmospheric teleconnections from the equatorial Pacific. *Mon. Wea. Rev., 97*, 163-172.

Bottomley, M., C.K. Foiland, J. Hsiung, R.E. Newell, and D.E. Parker, Global Ocean Surface Temperature Atlas, Her Majesty's Stn. Off., Norwich, England, 1990

Burgman, Robert J., Paul S. Schopf, Ben P. Kirtman, 2008: Decadal Modulation of ENSO in a Hybrid Coupled Model. *J. Climate*, **21**, 5482–5500.

Cane, M.A., S.E. Zebiak (1985), A Theory for El Niño and the Southern Oscillation. *Science, 228*(4703), 1085-1087, doi: 10.1126/science.228.4703.1085

Deser, C., Phillips, A. S., & Alexander, M. A. (2010), Twentieth century tropical sea surface temperature trends revisited. *Geophysical Research Letters*, *37*(L10701), doi: 10.1029/2010GL043321.

Folland, C. K. and Parker, D. E. (1995), Correction of instrumental biases in historical sea surface temperature data. *Q.J.R. Meteorol. Soc.,* 121: 319–367. doi: 10.1002/qj.49712152206.

Galanti, E., & Tziperman, E. (2000). Enso's phase locking to the seasonal cycle in the fast-sst, fast-wave, and mixed-mode regimes. *Journal of the Atmospheric Sciences*, *57*(17), 2936-2950.

Gill, A. E. (1982), *Atmosphere-ocean dynamics*. (p. 662). London: Academic Press.

Jin, Fei-Fei, 1997: An Equatorial Ocean Recharge Paradigm for ENSO. Part I: Conceptual Model. *J. Atmos. Sci.*, **54**, 811–829. doi: http://dx.doi.org/10.1175/1520-0469(1997)054<0811:AEORPF>2.0.CO;2

Kao, H.-Y., and J.-Y. Yu (2009), Contrasting Eastern-Pacific and Central-Pacific Types of ENSO. *J. Climate*, **22**, 615–632. doi: /10.1175/2008JCLI2309.1.

Kaplan, A., Y. Kushnir, M. A. Cane, and M. B. Blumenthal (1997), Reduced space optimal analysis for historical data sets: 136 years of Atlantic sea surface temperatures, *J. Geophys. Res., 102(C13),*27835–27860, doi:10.1029/97JC01734.

Kaplan, A., M. A. Cane, Y. Kushnir, A. C. Clement, M. B. Blumenthal, and B. Rajagopalan (1998), Analyses of global sea surface temperature 1856–1991, J. Geophys. Res., *103*, 18,567–18,589, doi:10.1029/97JC01736.

Kirtman, B. P., and P. S. Schopf, 1998: Decadal variability of ENSO predictability and prediction. *J. Climate*, **11,** 2804–2822.

Kug, J., Jin, F., and An, S. (2009). . Two types of el niño events: Cold tongue el niño and warm pool el niño, *Journal of Climate*, *22*(6), 1499-1515. doi: 10.1175/2008JCLI2624.1.

Lee, T., and M. J. McPhaden (2010), Increasing intensity of El Niño in the central-equatorial Pacific, *Geophys. Res. Lett., 37*, L14603, doi:10.1029/2010GL044007.

McPhaden, M. J., T. Lee, and D. McClurg (2011), El Niño and its relationship to changing background conditions in the tropical Pacific Ocean, *Geophys. Res. Lett., 38*, L15709, doi:10.1029/2011GL048275.

Minobe, S., and A. Maeda (2005), A 1 degree SST dataset compiled from ICOADS from 1850 to 2002 and Northern Hemisphere frontal variability, *Int. J. Climatol.*, **25**, 881–894, doi:10.1002/joc.1170.

Mo, K. C., Schemm, J. K. E., & Yoo, S. H. (2009). Influence of enso and the atlantic multidecadal oscillation on drought over the united states. *Journal of Climate*, *22*(22), 5962-5982.

Newman, M., S.-I. Shin, and M. A. Alexander (2011), Natural variation in ENSO flavors. *Geophys. Res. Lett., 38*, L14705, doi:10.1029/2011GL047658.

Penland, C., and P. D. Sardeshmukh, 1995: The optimal growth of tropical sea surface temperature anomalies. *J. Climate*, **8,** 1999–2024.

Philander, S. G. H., T. Yamagata and R. C. Pacanowski (1984). Unstable air-sea interactions in the tropics. *J. Atmos. Sci., 41*, 603-612.

Ping, C., J. Link, L. Hong, and M. Flugal, 1996: Chaotic dynamics versus stochastic processes in El Niño–Southern Oscillation in coupled ocean–atmosphere models. *Physica D*, **98,** 301–320.

Picaut, J., F. Maisa, Y. du Penhoat (1997), An Adevective-Reflective Conceptual Model for the Oscillatory Nature of the ENSO. *Science, 277*(5326), 663-666, doi: 10.1126/science.277.5326.663

Rayner, N. A., D. E. Parker, E. B. Horton, C. K. Folland, L. V. Alexander D. P. Rowell, E. C. Kent, and A. Kaplan (2003), Global analyses of sea surface temperature, sea ice,

and night marine air temperature since the late nineteenth century, J. Geophys. Res., 108(D14), 4407, doi:10.1029/ 2002JD002670.

Rayner, N. A., P. Brohan, D. E. Parker, C. K. Folland, J. J. Kennedy, M. Vanicek, T. J. Ansell, and S. F. B. Tett (2006), Improved Analyses of Changes and Uncertainties in Sea Surface Temperature Measured In Situ since the Mid-Nineteenth Century: The HadSST2 Dataset. *J. Climate*, **19**, 446–469.
doi: 10.1175/JCLI3637.1

Sheinbaum, J. (2003), Current theories on el niño-southern oscillation: A review. *Geofísica Internacional*,*42*(3), 291-305.

Smith, T. M., et al. (2008), Improvements to NOAA's historical merged land-ocean surface temperature analysis (1880–2006), *J. Clim., 21*, 2283–2296, doi:10.1175/2007JCLI2100.1.

The International Research Institute for Climate and Society. (n.d.). Retrieved from http://iri.columbia.edu/climate/ENSO/theory/index.html

Trenberth, K. E., and D. P. Stepaniak (2001), Indices of El Niño Evolution. *Journal of Climate*, **14(8)**, 1697–1701.

Trenberth, K. E. (1997), The definition of el niño. *Bulletin of the American Meteorological Society*, *78*(12), 2771-2777.

Walker, G. T. and E. Bliss (1932), World Weather V. Mem, *Roy Met. Soc., 4*, 53-84.

Wang, C. (2001), On the ENSO mechanisms. *Advances in Atmospheric Sciences*, *18*(5), 674-691.

Wu, B., Li, T., & Zhou, T. (2010), Asymmetry of atmospheric circulation anomalies over the western north pacific between el niño and la niña. *Journal of Climate*, *23*(18), 4807-4822.

Yeh, S.-W., J.-S. Kug, B. Dewitte, M.-H. Kwon, B. Kirtman, and F.-F. Jin (2009), El Niño in a changing climate, *Nature, 461*, 511–514, doi:10.1038/nature08316.

Yeh, S.-W., B. P. Kirtman, J.-S. Kug, W. Park, and M. Latif (2011), Natural variability of the central Pacific El Niño event on mulit-centennial timescales, *Geophys. Res. Lett., 38,* L022704, doi: 10.1029/2010GL045886.

Yu, J.-Y. and S. T. Kim (2010), Three evolution patterns of Central-Pacific El Niño, *Geophys. Res. Lett., 37,* L08706, doi:10.1029/2010GL042810.

Yu, J.-Y., Y. Zou, S. T. Kim, and T. Lee (2012), The changing impact of El Niño on US winter temperatures, *Geophys. Res. Lett., 39*, L15702, doi:10.1029/2012GL052483.

Zebiak, S. E., 1989: On the 30–60 day oscillation and the prediction of El Niño. *J. Climate*, **2,** 1381–1387.

APPENDIX

Niño 3:

(a)

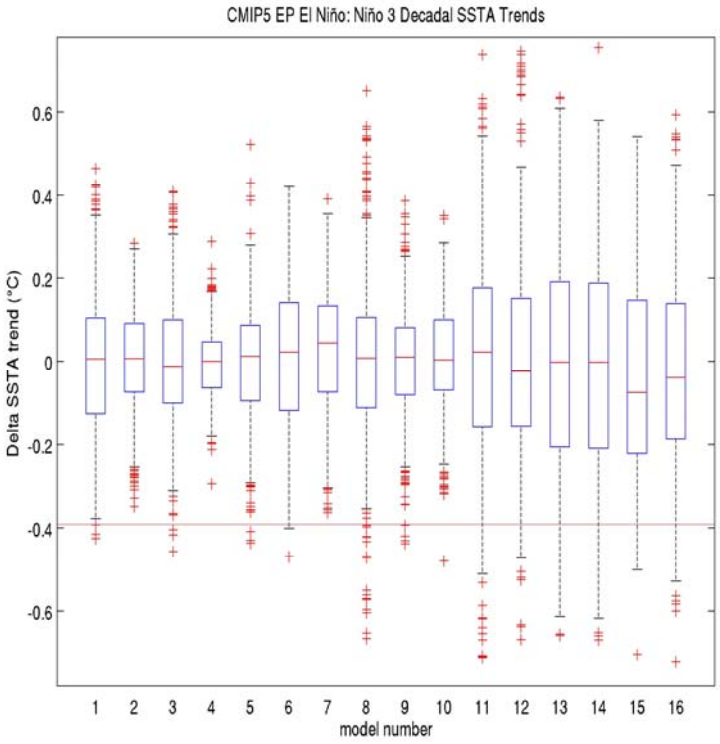

-Lee and McPhaden (2010)
Niño 3 trend= -0.39 °C

(b)

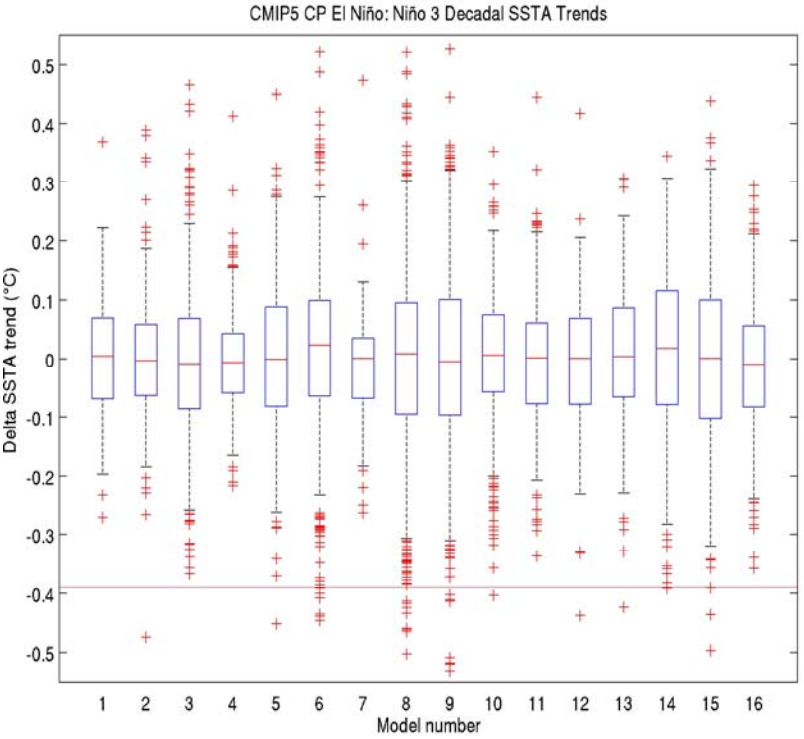

-Lee and McPhaden (2010)
Niño 3 trend= -0.39 °C

Niño 4:

(c)

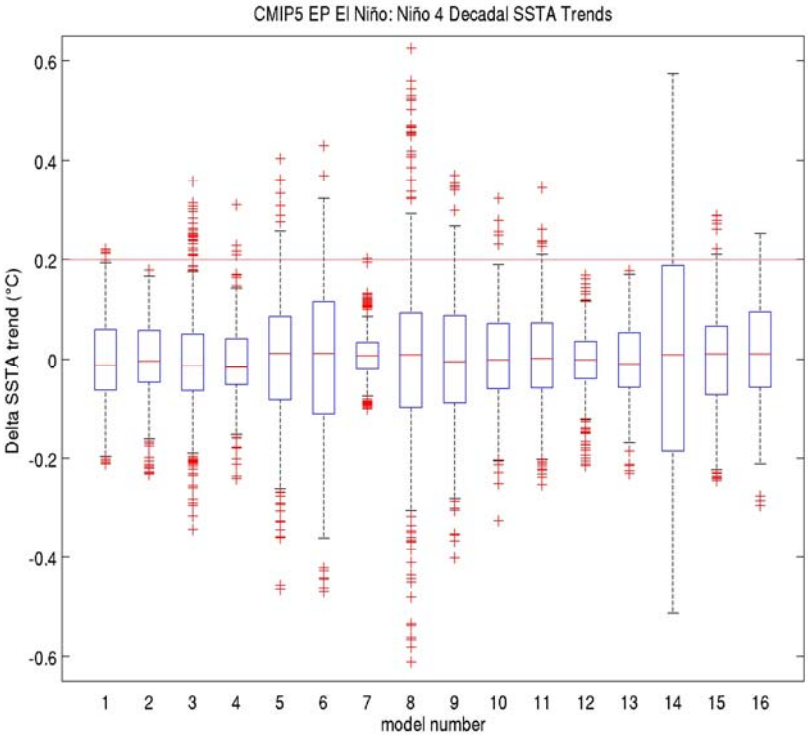

-Lee and McPhaden (2010) Niño 4 trend =0.20 °C

(d)

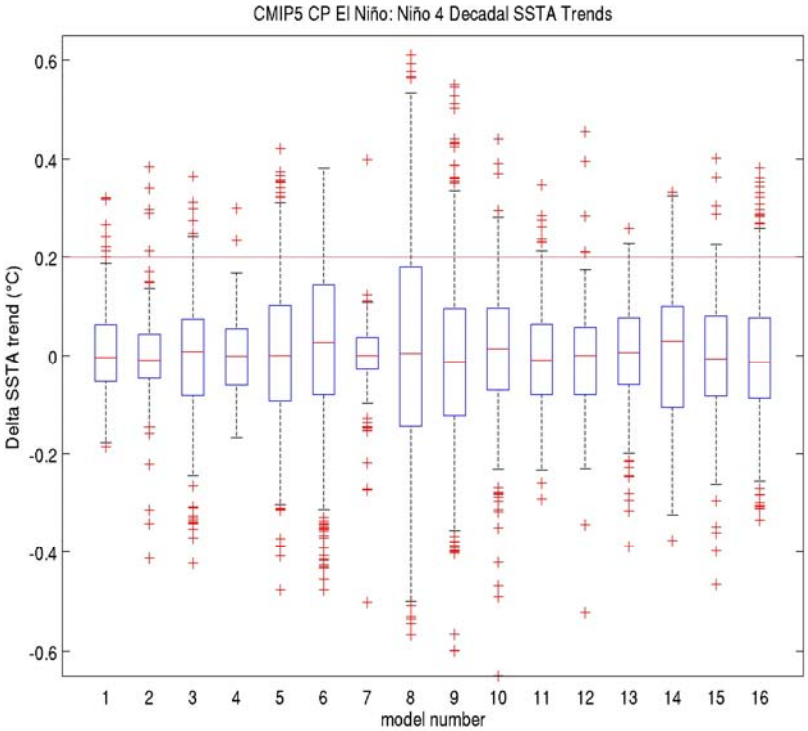

-Lee and McPhaden (2010) Niño 4 trend =0.20 °C

Figure 15. (a) CMIP5 EP El Niño: Niño 3 Decadal SSTA Trends (b) CMIP5 CP El Niño: Niño 3 Decadal SSTA Trends (c) CMIP5 EP El Niño: Niño 4 Decadal SSTA Trends (d) CMIP5 CP El Niño: Niño 4

Decadal SSTA Trends. Distributions of SSTA trends for CMIP5 piControl runs for (a.) EP Niño 3 (b.) CP Niño 3 (c) EP Niño 4 (d) CP Niño 4. Model numbers refer to Table 4. The trend result for Lee and McPhaden [2010] is plotted on the Niño 3 and 4 figures to compare with model results. Each Figure is described as such: Red lines denote the mean surrounded by a blue box signifying the 1st quartile, with arms extending to 1.96σ or 95% CI.